Western Arabian Sea SST during the penultimate interglacial: A comparison of U-37(K ') and Mg/Ca paleothermometry

Western Arabian Sea SST during the penultimate interglacial: A comparison of $U^{K'}_{37}$ and Mg/Ca paleothermometry

M. H. Saher,[1,2] F. Rostek,[3] S. J. A. Jung,[1,4] E. Bard,[3] R. R. Schneider,[5] M. Greaves,[6] G. M. Ganssen,[1] H. Elderfield,[6] and D. Kroon[1,4]

Received 9 October 2007; revised 15 February 2009; accepted 27 February 2009; published 29 May 2009.

[1] Millennial-scale records of planktonic foraminiferal Mg/Ca, bulk sediment $U^{K'}_{37}$, and planktonic foraminiferal $\delta^{18}O$ are presented across the last two deglaciations in sediment core NIOP929 from the Arabian Sea. Mg/Ca-derived temperature variability during the penultimate and last deglacial periods falls within the range of modern day Arabian Sea temperatures, which are influenced by monsoon-driven upwelling. The $U^{K'}_{37}$-derived temperatures in MIS 5e are similar to modern intermonsoon values and are on average 3.5°C higher than the Mg/Ca temperatures in the same period. MIS 5e $U^{K'}_{37}$ and Mg/Ca temperatures are 1.5°C warmer than during the Holocene, while the $U^{K'}_{37}$-Mg/Ca temperature difference was about twice as large during MIS 5e. This is surprising as, nowadays, both proxy carriers have a very similar seasonal and depth distribution. Partial explanations for the MIS 5e $U^{K'}_{37}$-Mg/Ca temperature offset include carbonate dissolution, the change in dominant alkenone-producing species, and possibly lateral advection of alkenone-bearing material and a change in seasonal or depth distribution of proxy carriers. Our findings suggest that (1) Mg/Ca of *G. ruber* documents seawater temperature in the same way during both studied deglaciations as in the present, with respect to, e.g., season and depth, and (2) $U^{K'}_{37}$-based temperatures from MIS 5 (or older) represent neither upwelling SST nor annual average SST (as it does in the present and the Holocene) but a higher temperature, despite alkenone production mainly occurring in the upwelling season. Further we report that at the onset of the deglacial warming, the Mg/Ca record leads the $U^{K'}_{37}$ record by 4 ka, of which a maximum of 2 ka may be explained by postdepositional processes. Deglacial warming in both temperature records leads the deglacial decrease in the $\delta^{18}O$ profile, and Mg/Ca-based temperature returns to lower values before $\delta^{18}O$ has reached minimum interglacial values. This indicates a substantial lead in Arabian Sea warming relative to global ice melting.

Citation: Saher, M. H., F. Rostek, S. J. A. Jung, E. Bard, R. R. Schneider, M. Greaves, G. M. Ganssen, H. Elderfield, and D. Kroon (2009), Western Arabian Sea SST during the penultimate interglacial: A comparison of $U^{K'}_{37}$ and Mg/Ca paleothermometry, *Paleoceanography*, *24*, PA2212, doi:10.1029/2007PA001557.

1. Introduction

[2] Knowledge of sea surface temperature (SST) variations is pivotal for climate reconstructions. A number of SST proxies have been developed, including isotopic ($\delta^{18}O$) and elemental composition (Mg/Ca) of calcareous microfossils, and the chemistry of organic constituents produced in surface waters (e.g., $U^{K'}_{37}$ and TEX_{86}). The resulting SST estimates may differ, however, as the various proxy carriers each have their particular seasonal distribution, depth habitat, and preservation potential.

[3] Producing more than one temperature proxy record on the same material allows assessment of the nature and magnitude of these differences [*Bard*, 2001a; *Mix et al.*, 2000; *Mollenhauer et al.*, 2003; *Nürnberg et al.*, 2000]. Here we address this proxy specific temperature sensitivity by comparing alkenone- and Mg/Ca-derived SST estimates, using downcore sediments from the western Arabian Sea (Core NIOP929; Figure 1). When interpreting downcore proxy records it is vital to know if, and how, the documentation of the desired variable by the proxy carrier has changed through time.

[4] In the Arabian Sea, monsoon controlled seasonal upwelling of cold subsurface water results in strong vertical and seasonal temperature gradients in the upper water column. Our aims were (1) to document the derived temperature histories across the last two deglaciations at the millennial timescale; (2) to understand the specific temperature signature of the proxies used by comparing the results to modern seasonal temperature variability in the upper water column; and (3) to document the phasing

[1]Department of Paleoclimatology and Geomorphology, Institute of Earth Sciences, Vrije Universiteit Amsterdam, Amsterdam, Netherlands.
[2]Now at Norwegian Polar Institute, Polar Environment Centre, Tromsø, Norway.
[3]CEREGE, UMR6635, Aix-Marseille Université, IRD, Collège de France, CNRS, Aix-en-Provence, France.
[4]Now at John Murray Laboratories, School of GeoSciences, University of Edinburgh, Edinburgh, UK.
[5]Institute of Geosciences, Christian Albrechts University of Kiel, Kiel, Germany.
[6]Department of Earth Sciences, University of Cambridge, Cambridge, UK.

0883-8305/09/2007PA001557

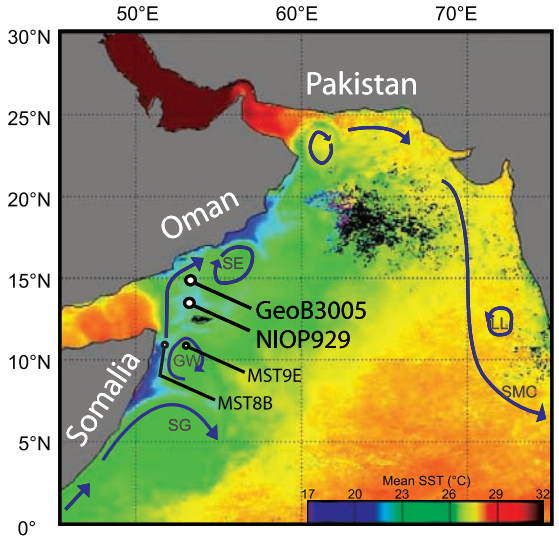

Figure 1. The Arabian Sea with the locations of cores NIOP929 and GeoB3005. Colors indicate mean July temperature. Surface currents are indicated. SG, southern gyre; GW, great whirl; SE, Socotra Eddy; LL, Laccadive low; SMC, Southwest Monsoon Current. SST information by NASA. Currents modified after *Schott and McCreary* [2001], with permission from Elsevier.

between the various temperature proxy records, and the possible effect of bioturbation on this.

2. Hydrography and Modern Calcification Temperatures of *G. ruber* and *E. huxleyi*

[5] In order to provide a background for the interpretation of our paleotemperature records, we first evaluate modern day calcification temperatures for our proxy carriers in the study area. Both *G. ruber* (Mg/Ca) and *E. huxleyi* ($U^{K'}_{37}$) are reported to live mainly in the upper 50 m (mixed layer) of the water column [*Peeters et al.*, 2002; *Andruleit et al.*, 2003]. Annual average temperature for the upper 50 m in the Arabian Sea is ~26°C [*Levitus et al.*, 1994], with maximum average monthly values of ~28°C in May, during the intermonsoon period, and lowest average temperatures of ~23°C, during the upwelling season (Figure 2). In situ (not averaged) measurements near site NIOP 929 show temperatures as low as 20°C during the upwelling season [*Brummer et al.*, 2002]. In the more stable nonupwelling season the differences between the data sets are minor.

[6] Combining these temperature [*Levitus et al.*, 1994; *Brummer et al.*, 2002] and depth [*Peeters et al.*, 2002; *Andruleit et al.*, 2003] data with flux data of the proxy carriers from nearby sediment traps [*Conan and Brummer*, 2000; *Curry et al.*, 1992] we calculated an annual average calcification temperature of 24–25.4°C for *G. ruber*, and 24.5°C to 25°C for coccolithophorids. In an earlier study *Rostek et al.* [1997], on the basis of data from *Ittekkot et al.* [1992] calculated a slightly higher flux-weighted coccolithophore calcification temperature of 25.7°C. The difference can be explained by the use of water temperatures at 10 m depth [*Rostek et al.*, 1997] instead of 0–50 m (this study).

3. Material and Methods

[7] Core NIOP929 (Figure 1) was recovered from the western Arabian Sea (13°42, 21N; 53°14,76E) at 2490 m water depth, as part of the Netherlands Indian Ocean Programme [*van Hinte et al.*, 1995]. The core consists of moderately bioturbated, greenish calcareous ooze.

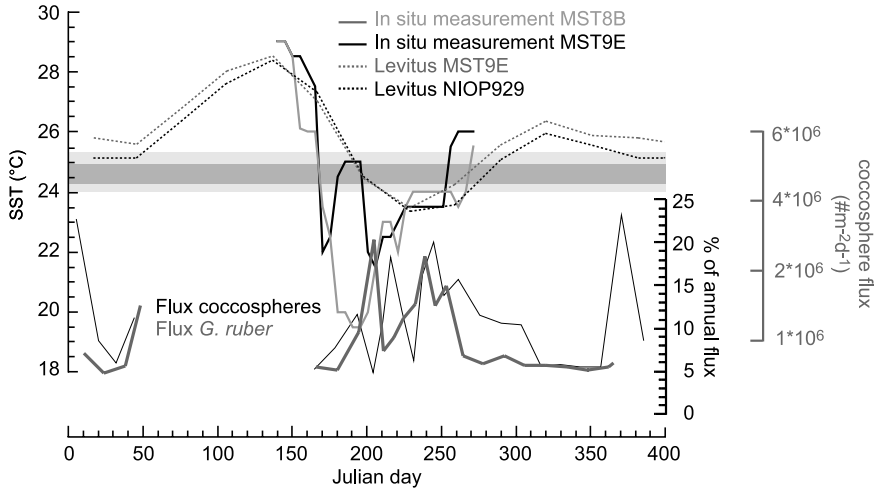

Figure 2. Temperature time series [*Brummer et al.*, 2002; *Levitus et al.*, 1994] from the locations of Core NIOP929 and nearby sediment traps MST9E and MST8B (Figure 1). Data on foraminifera and coccosphere flux were taken from MST9E. Also shown are the flux of *G. ruber* as a percentage of total measured annual flux [*Conan and Brummer*, 2000] and coccosphere flux in specimens/d/m^2 for MST9E [*Broerse et al.*, 2000]. Notice that the *Levitus et al.* [1994] temperatures are monthly averages over a 1°C × 1°C × 50 m volume. The horizontal gray bars indicate modern flux-weighted average annual calcification temperatures for *G. ruber* (light gray) and coccolithophores (dark gray) at the given locations.

Table 1. Age/Depth Tie Points for the MIS 6–5 Section of Core NIOP929

Depth (cm)	Age (ka B.P.)
883.5	96.38
903.5	99.96
930.5	107.55
997.5	123.82[a]
1044.5	131.09
1067.5	135.34
1175.5	149.34

[a]Isotopic event 5.5.

[8] An overall age model is taken from *Rostek et al.* [1997], who indicated that the 16.15 m long sediment core covers the last 240 ka. *Rostek et al.* [1997] provide medium resolution $\delta^{18}O_{(N.\ dutertrei)}$ and alkenone SST records, produced using methods similar to those in this study, for the entire core. An updated chronology for the last 20 ka B.P., based on seven ^{14}C datings, as well as the high-resolution $\delta^{18}O$ and Mg/Ca data, have been taken from *Saher et al.* [2007a]. This interval has an average temporal resolution of 50 years.

[9] For the present paper we sampled the interval 870.5–1191.5 cm, covering the previous glacial-interglacial transition, at a millennial-scale (1 cm) resolution. The age model for this core section was improved by aligning the high-resolution $\delta^{18}O_{(G.\ ruber)}$ profile with the SPECMAP $\delta^{18}O$ stack [*Martinson et al.*, 1987], using seven tie points (Table 1 and Figure 4). Average temporal resolution for this interval is 180 years.

[10] Samples for alkenone unsaturation ($U^{K'}_{37}$) were taken separately from those for $\delta^{18}O$ and Mg/Ca. The sample slices used for $\delta^{18}O$ and Mg/Ca were freeze-dried and wet sieved over a 63 μm sieve. Fifty tests of *G. ruber* were picked from the 250–355 μm fraction; 20 specimens were used for Mg/Ca measurements, and 30 for stable isotope measurements.

[11] For stable isotope measurements, the tests of *G. ruber* were crushed, and ~30 μg was measured in a Finnigan MAT252 equipped with a Kiel device. The long-term external reproducibility of the $\delta^{18}O$ measurements on a laboratory standard is ±0.08‰. All isotope measurements were performed at the Institute of Earth Sciences, Vrije Universiteit, Amsterdam.

[12] The Mg/Ca measurements were performed on a 3 cm resolution. For the Mg/Ca measurements 20 tests of *G. ruber* were gently crushed between glass plates, and subjected to a cleaning process designed to remove all clay and organic matter (method after *Barker et al.* [2003]). After dissolution in 350 μl HNO_3, the samples were additionally centrifuged for 5 min at 5000 rpm to settle any remaining small silicate particles. Approximately 300 μl (residue free) aqueous solution was analyzed on a Varian Vista AX at the Department of Earth Sciences at Cambridge University (see for details *de Villiers et al.* [2002]). Mg/Ca ratios were converted to temperature estimates using the equation by *Anand et al.* [2003]: $Mg/Ca = 0.34 \exp(0.102T)$. This specific equation was chosen because *Anand et al.* [2003] used foraminifera tests from a very similar size fraction, and subjected these to a cleaning method very similar to that used in this study.

[13] Alkenone unsaturation ratio ($U^{K'}_{37}$) and total C_{37} measurements were performed on freeze-dried bulk samples at CEREGE (Aix-en-Provence, France) at a 3 cm resolution (Figure 3). For a detailed description of the methods, see *Sonzogni et al.* [1997a]. Precision and accuracy were checked during an international intercomparison involving ca. 30 laboratories [*Rosell-Melé et al.*, 2001]. The alkenone unsaturation ratios were transferred to temperature using the equation for temperatures in the range 24–29°C by *Sonzogni et al.* [1997b]: $U^{K'}_{37} = 0.316 + 0.023T$. This calibration is based on low-latitude core tops from the Indian Ocean. This equation has a reduced slope (0.024/°C) when compared to the linear equation (0.033/°C) based on core tops compiled from all oceans [*Müller et al.*, 1998]. This compilation, as well as culture studies using different strains of *Gephyrocapsa oceanica* and *Emiliania huxleyi* [*Conte et al.*, 1998] and measurements on sinking particulate matter from Bermuda [*Conte et al.*, 2001], strongly suggest that the shape of the $U^{K'}_{37}$ versus temperature relation is sigmoidal; that is, the $U^{K'}_{37}$ index converges asymptotically toward 0 and 1, for low and high temperatures, respectively [*Conte et al.*, 2006]. In Figure 3 we also provide temperature estimates calculated using the linear equation by *Prahl and Wakeham* [1987], which is based on a culture of *E. huxleyi*, between 10 and 25°C, and thus might not be suitable for the high SST of the western equatorial Arabian Sea. The equation by *Prahl and Wakeham* [1987] is generally used as the standard one, and it is indistinguishable from the global core top calibration of *Müller et al.* [1998].

[14] We further established average test weight of the *G. ruber* frustules within a narrow size range. The 250–300 μm fraction was counted and weighed on a Sartorius microbalance (micro M 3 P) with a precision of 0.001 mg. The resultant test weight represents an average value for a population of on average 22 tests. In the interval 940 to 980 cm, scarcity of *G. ruber* limited the number of Mg/Ca and test weight measurements. After weighing and before chemical analysis, the 250–300 μm and 300–355 μm fractions were recombined, in order to use the same size fraction in the physical and chemical analyses as previous studies [e.g., *Peeters et al.*, 2002; *Saher et al.*, 2007a].

4. Results

4.1. Results From Core NIOP929

[15] The stable oxygen isotope record of *G. ruber* from Core NIOP929 (Figure 4) shows maximum values of ~0.1‰ at 152 and 135 ka B.P., and minimum values of −2.2‰ around 124 ka B.P. The high MIS 6 $\delta^{18}O$ values are followed by three light pulses, prior to the onset of the deglaciation. A short-lived $\delta^{18}O$ minimum demarcates MIS 5e at the end of Termination II. Subsequently, higher (−0.9‰) values prevail during MIS 5d, followed by two local $\delta^{18}O$ minima, reaching minimum values of ~−1.3‰ during MIS 5c.

[16] The shell weight record (Figure 3) is fairly constant, with slightly lower than average values around 1000 cm depth, and large variability at 870–990 cm depth, an interval with low sample resolution due to limited availability of foraminifera tests. The average shell weight is 10.4 μg.

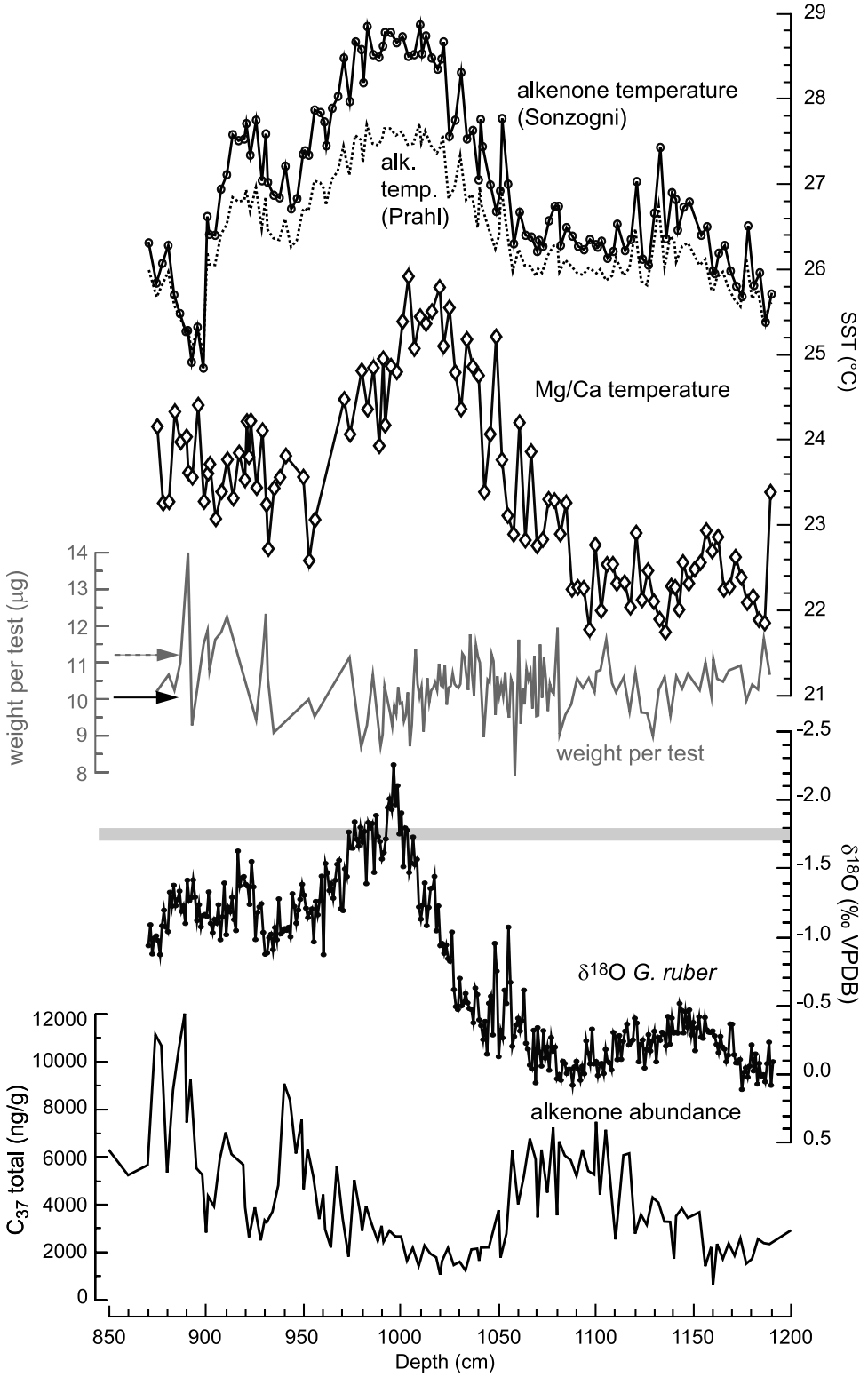

Figure 3. The Core NIOP929 alkenone ($U^{K'}_{37}$) SST record, calculated using the transfer functions by *Sonzogni et al.* [1997b] (line with open circles) and by *Prahl and Wakeham* [1987] (dotted line), the Mg/Ca SST (line with diamonds) record (equation from *Anand et al.* [2003]; record not corrected for carbonate dissolution), average test weight (gray line), the $\delta^{18}O$ record of *G. ruber* (line with solid circles), and the C_{37} abundance (solid black line) records plotted against depth. The horizontal gray line indicates modern day average $\delta^{18}O$ [*Conan and Brummer*, 2000]. The black arrow indicates the average value of the shell weight data. The gray arrow shows the average shell weight of the LGM-Holocene section of the same core [*Saher et al.*, 2007a].

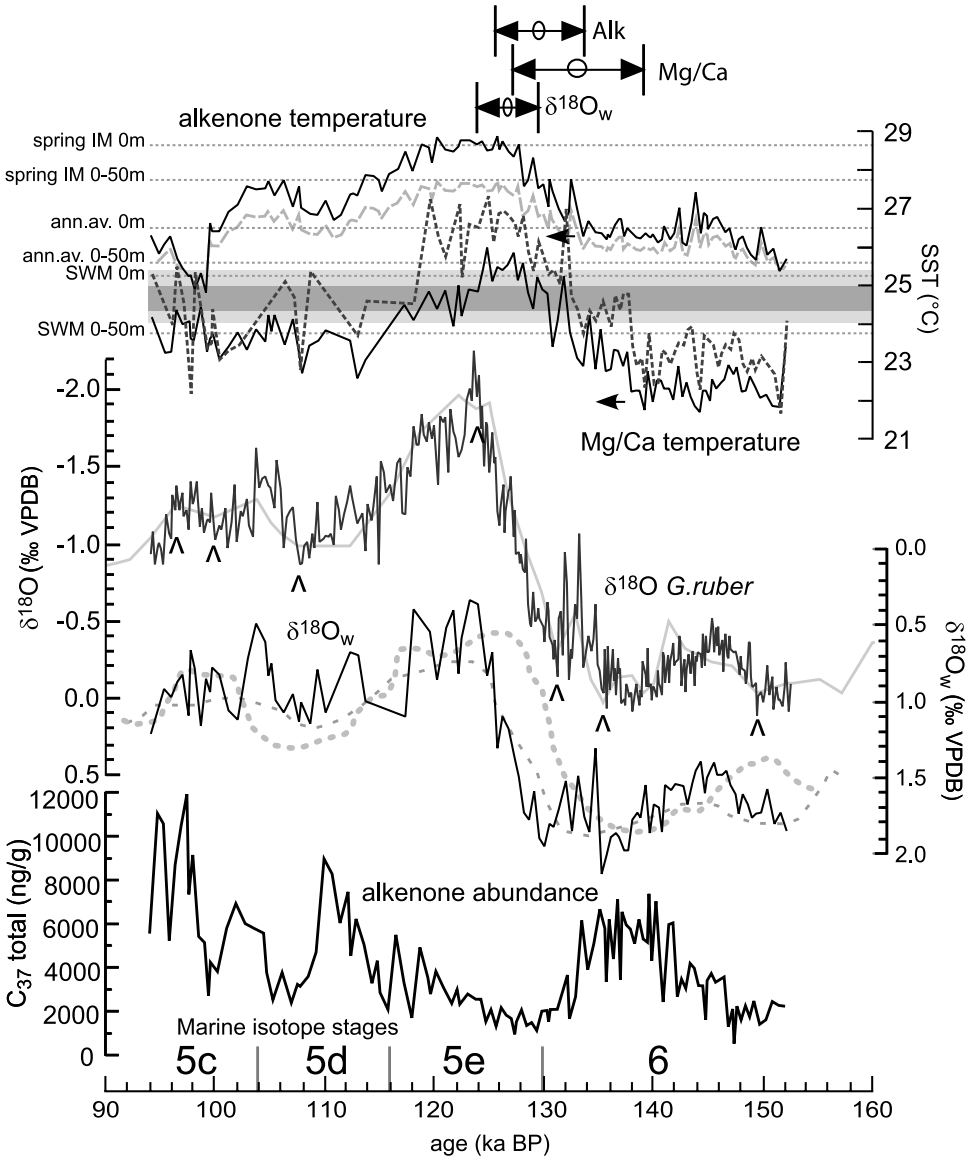

Figure 4. The Core NIOP929 alkenone (solid black line, transfer function by *Sonzogni et al.* [1997b]; dashed gray line, transfer function by *Prahl and Wakeham* [1987]) and Mg/Ca-based (solid black line) SST reconstructions plotted with the δ^{18}O *G. ruber* (solid dark gray line) and $\delta^{18}O_w$ (solid black line) for the isotope stage 6–5 time interval. Superimposed on the NIOP929 δ^{18}O record is the SPECMAP δ^{18}O stack on an arbitrary vertical scale (solid light gray line). Tie points are indicated by black arrowheads. Vertical scale is such that 1‰ in NIOP929 δ^{18}O corresponds with 4°C. Added in is the Mg/Ca SST record (dashed gray line), corrected for dissolution, using the equation by *Rosenthal and Lohmann* [2002]. Superimposed on the $\delta^{18}O_w$ record are two global oceanic $\delta^{18}O_w$ reconstructions, from *Shackleton* [2000] (thick dashed line) and *Waelbroeck et al.* [2002] (thin dashed line). Horizontal gray bars indicate modern flux-weighted average annual calcification temperature for *G. ruber* (light gray) and coccolithophores (dark gray) in the western Arabian Sea. Calcification temperatures are calculated using temperature data from *Levitus et al.* [1994] and flux data from *Curry et al.* [1992], *Broerse et al.* [2000], and *Conan and Brummer* [2000]. Dashed horizontal lines indicate modern average values for the temperature at the surface and in the upper 50 m of the water column during the spring intermonsoon season (spring IM), the whole year (ann. av.), and the summer monsoon season (SWM) at the location of core NIOP929 as derived from the *Levitus et al.* [1994] atlas. Single-headed arrows indicate onset of early warming in the SST records, and double-headed arrows indicate duration and midpoint of the termination in the SST and $\delta^{18}O_w$ records. Marine isotope stages are indicated at the bottom.

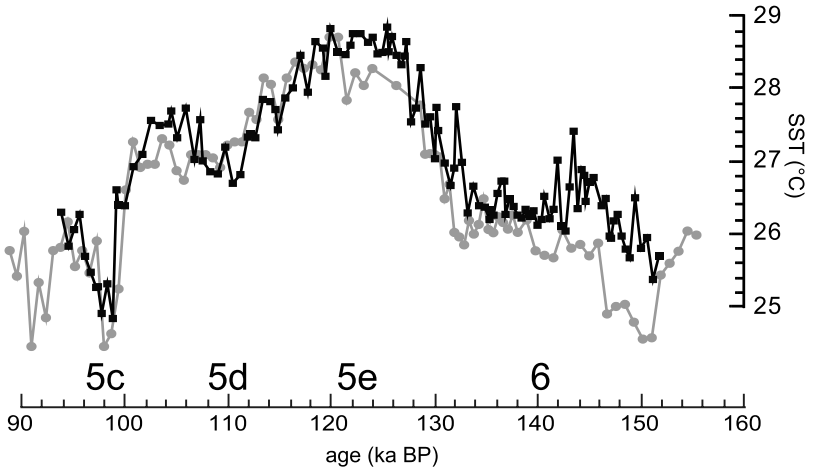

Figure 5. The alkenone ($U_{37}^{K'}$) SST records of cores NIOP929 (black, transfer function by *Sonzogni et al.* [1997b]) and GeoB3005 (gray, same transfer function) tuned to the same timescale.

[17] The Mg/Ca-based temperature record, which has an average sample spacing of 540 years (Figure 4), shows rapid high-amplitude fluctuations of up to 2.4°C in several hundred years. The temperatures during peak MIS 6 oscillated around 22°C. Between 138 and 125 ka B.P., temperature gradually increased toward a maximum value of 26°C in MIS 5e, which is slightly warmer than present. Superimposed, rapid temperature variations occur during the deglacial warming. The high temperatures of MIS 5e were maintained for ~4000 years, followed by a drop in temperature to below 23°C in MIS 5d. During MIS 5c temperatures of ~24°C prevailed.

[18] The $U_{37}^{K'}$-based temperature record, which has an average sample spacing of 470 years (Figure 4), shows temperatures between 25.5°C and 27.5°C in MIS 6, with a local maximum at ~144 ka B.P. The onset of the deglacial warming occurred at 134 ka B.P., i.e., ~4000 years later than indicated in the Mg/Ca data. The deglacial temperature rise shows large fluctuations, and resulted in maximum temperatures of almost 29°C at 128 ka B.P. $U_{37}^{K'}$ temperature exceeded 28.5°C for ~10,000 years, and then dropped to 27°C in MIS 5d. During MIS 5c, temperature returned to ~28°C, followed by a sharp drop to 25°C. These cold conditions prevailed for a few thousand years, followed by a temperature rise to > 26°C.

[19] The C_{37} abundance (Figure 4) shows minimum values during the deglaciation and MIS 5e, when temperature was highest, and maximum values in late stage 6 and during two periods of several thousand years in MIS 5d and 5c.

[20] To test whether the $U_{37}^{K'}$ results of Core NIOP929 are robust on a regional scale, these results are compared with data from nearby core GeoB3005 (14°58′N, 53°22′E; 2316 m depth; Figure 1 [*Budziak*, 2001]). In order to align the records from both cores, the GeoB3005 $\delta^{18}O_{(N.\ dutertrei)}$ record was tuned to the NIOP929 $\delta^{18}O_{(G.\ ruber)}$ record (not shown). Comparison of the $U_{37}^{K'}$ time series of both cores confirms that these are largely similar, both in timing and in amplitude (Figure 5). Slightly lower temperatures at 152–143 ka B.P., and during MIS 5e, may be explained by the location of core GeoB3005 being more proximal to the center of the coastal upwelling area offshore Yemen. The occurrence of a pronounced temperature minimum of about 2°C around 98 ka B.P. in both records indicates that this event is not an artifact.

[21] The results from the upper portion of the core, covering the last deglaciation to late Holocene, are taken from *Saher et al.* [2007a] and are not described here.

4.2. Comparison of 152–94 ka B.P. Temperatures With Modern Day SSTs

[22] In the western Arabian Sea, Mg/Ca-derived temperatures in MIS 5e (Figure 4) are slightly higher than the calculated modern calcification temperatures of *G. ruber* of ~25°C (Figure 2). These high temperatures correspond to lighter than modern $\delta^{18}O$ values of *G. ruber*. Holocene Mg/Ca and $\delta^{18}O$ measurements [*Saher et al.*, 2007a] are similar to modern values. The (coccolithophore controlled) $U_{37}^{K'}$ temperature estimate of the core top is higher than the coccolithophore (*E. huxleyi*) calcification temperature of 24.5°C to 25°C calculated from sediment trap data by *Broerse et al.* [2000] (section 2). In Core NIOP929, $U_{37}^{K'}$-derived temperatures as low as this calculated calcification temperature are only found during the LGM, and during a few millennia around 98 ka B.P. During remaining periods, $U_{37}^{K'}$-based temperatures exceed the modern calcification temperature by 1–4°C. $U_{37}^{K'}$ temperature in the Holocene is close to the annual (not flux-weighted) average SST (Figure 6), as was already stated by *Rostek et al.* [1997], while it is close to the modern intermonsoon SST in MIS 5e.

4.3. Temperatures in the Period 152–94 ka B.P. Compared to the Last 20,000 Years

[23] When comparing the last with the penultimate glacial-interglacial transition, both Mg/Ca- and $U_{37}^{K'}$-based temperature estimates differ. While Mg/Ca data indicate similar SSTs during periods of maximum cold (late glacials), $U_{37}^{K'}$ results indicate a ~2.5°C warmer MIS 6 compared to the LGM. Both proxies consistently show 1.5°C higher temperatures

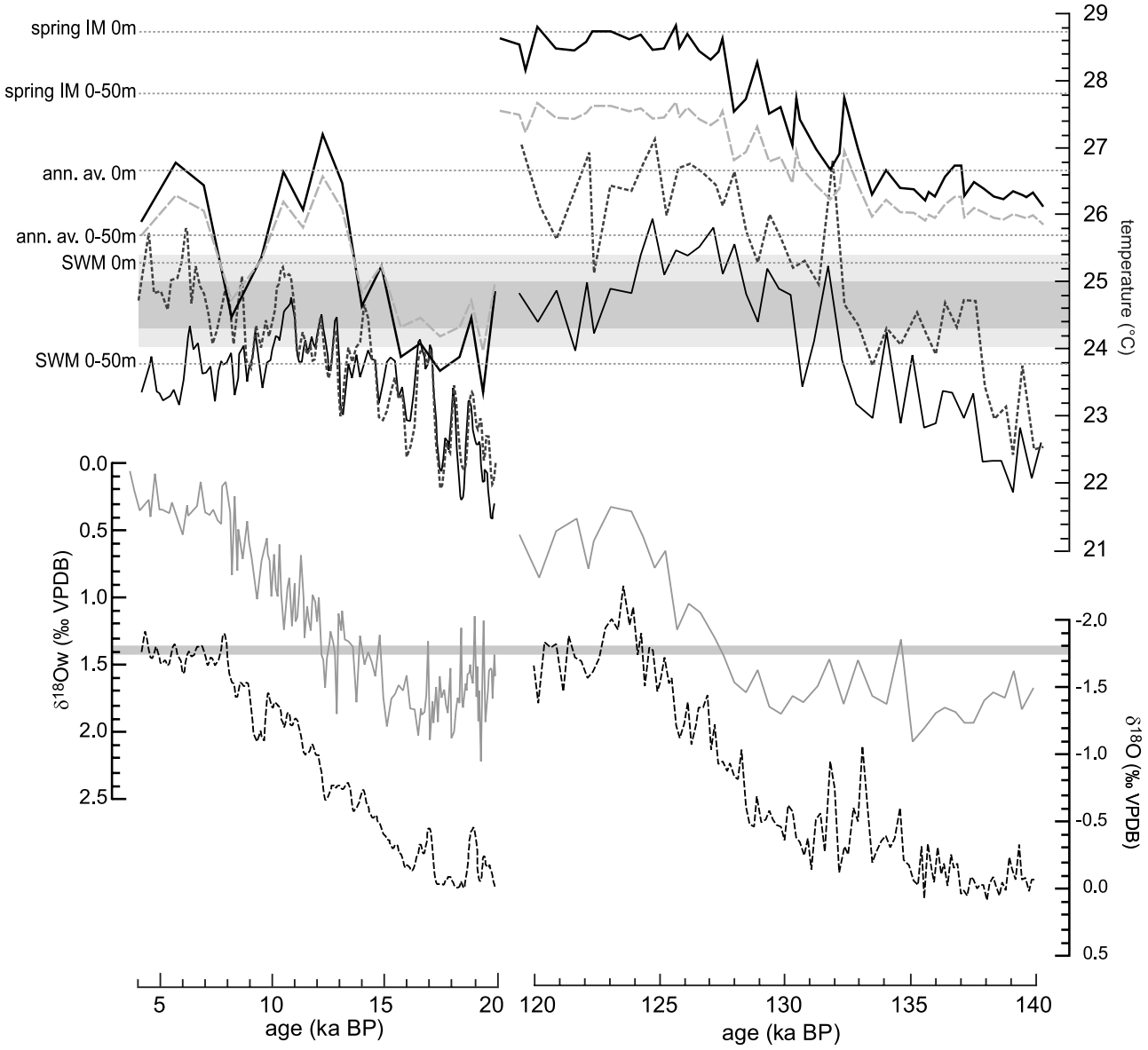

Figure 6. Comparison of the NIOP929 $\delta^{18}O$ and SST records from the last two glacial-interglacial cycles. From bottom to top: $\delta^{18}O_{(G.\ ruber)}$ (dashed black line), $\delta^{18}O_w$ (solid gray line), Mg/Ca-based SST reconstruction (thin solid black line), Mg/Ca-based SST corrected for dissolution by applying the equation by *Rosenthal and Lohmann* [2002] (dashed dark gray line), and alkenone-based SST reconstruction (thick solid black line, transfer function by *Sonzogni et al.* [1997b]; dashed light gray line, transfer function by *Prahl and Wakeham* [1987]). The data from the last 20,000 years are taken from *Saher et al.* [2007a] ($\delta^{18}O_w$), *Saher et al.* [2007b] ($\delta^{18}O_{(G.\ ruber)}$ and Mg/Ca SST both raw and corrected), and *Rostek et al.* [1997]. Dashed horizontal lines indicate modern average values for the temperature at the surface and in the upper 50 m of the water column during the spring intermonsoon season (spring IM), the whole year (ann. av.), and the summer monsoon season (SWM) at the location of core NIOP929 as derived from the *Levitus et al.* [1994] atlas. Gray areas depict modern flux-weighted average calcification temperatures of *G. ruber* (light gray) and coccolithophores (dark gray) as deduced from Figure 2.

during MIS 5e (Figures 4 and 6). $U^{K'}_{37}$-based temperature during MIS 5c range from low Holocene values to higher than Holocene values, whereas Mg/Ca data imply roughly modern day temperatures during this time interval.

[24] It is interesting to note that considerably higher $U^{K'}_{37}$ temperature estimates for the penultimate, compared to the last deglacial, cycle have also been documented from various locations outside the Arabian Sea [*Calvo et al.*, 2001;

Eglinton et al., 1992; *Hinrichs et al.*, 1997; *Schneider et al.*, 1996, 1999], placing this phenomenon on a global scale.

5. Discussion

5.1. Offset Between the $U_{37}^{K'}$- and Mg/Ca-Based Temperature Records

[25] The validity of derived temperature records depends on our understanding of the ecology of the proxy carrier, and how the signal may have been affected by secondary processes. When different techniques are applied to the same samples, differences between paleotemperature records provide clues to the underlying controls. The most striking difference between the $U_{37}^{K'}$-and Mg/Ca-based temperature records during MIS 6–5 is the average 3.5°C offset (Figure 4). This offset is not an artifact of the transfer function that was used to translate the alkenone unsaturation to temperature. When alternatively using the *Prahl and Wakeham* [1987] equation, the temperature offset decreases on average by only 0.3°C (max. 1.1°C, in MIS 5e) of the 3.5°C (Figure 3). Using a different conversion for Mg/Ca to temperature can work both ways; using the *Elderfield and Ganssen* [2000] equation, which is based on core tops, would only increase the temperature difference. Using the equation derived by *McConnell and Thunell* [2005] would reduce the temperature offset by 1.3°C; however, this equation is not preferred for our data because of the different methodology. Altogether, choice of transfer function affects the Mg/Ca-$U_{37}^{K'}$ temperature offset, but cannot explain it in total.

[26] Changes in surface ocean properties such as variations in salinity may affect paleotemperature estimates derived from Mg/Ca and $U_{37}^{K'}$ data. While Mg/Ca ratios may change in areas of high salinity variability [e.g., *Kisakurek et al.*, 2007; *Ferguson et al.*, 2008], in regions with minor salinity variation like the Arabian Sea this effect should be negligible. Currently, the effect of salinity variations on $U_{37}^{K'}$-based temperature estimates is debated, and estimates range from no change to a small influence at most [*Sonzogni et al.*, 1997a; *Blanz et al.*, 2005; *Liu et al.*, 2008]. We therefore assume that the temperature records have not been significantly affected by salinity variations.

[27] Alkenones have been reported to not be affected by seafloor processes, such as biodegradation [*Madureira et al.*, 1995; *McCaffrey et al.*, 1990; *Prahl et al.*, 1989]. Furthermore, the excellent agreement between the two alkenone records of cores NIOP929 and GeoB3005 measured in two different laboratories rules out an overestimation of the $U_{37}^{K'}$ temperature because of preferential degradation of the minor C37:3 alkenone.

[28] Changes in carbonate chemistry, specifically the carbonate ion effect, in the surface ocean may also affect the recording of temperature in the different proxy carriers. *Elderfield et al.* [2006], who studied the effect of $[CO_3^{2-}]$ on the Mg/Ca values of benthic foraminifera, point out that this effect is only important at temperatures below ~3°C. In addition, *Russell et al.* [2004] argue that foraminiferal Mg/Ca is only affected by $[CO_3^{2-}]$ at pH lower than at present. Given that the pCO_2 record of the Vostok ice core indicates that pH during the Quaternary has remained at above present-day levels [*Lea et al.*, 1999; *Petit et al.*, 1999] and that SST in the Arabian Sea are/were well above 3°C, we conclude that the Mg/Ca record of core NIOP929 has not been significantly affected by changes in $[CO_3^{2-}]$ concentration.

5.1.1. Mg/Ca and $U_{37}^{K'}$ Offset: Seasonal Distribution and Depth Habitat of Proxy Carriers

[29] Mg/Ca and $U_{37}^{K'}$ values are recorded by different organisms, which means that seasonal or depth habitat preferences of the respective proxy carrier may result in different SST estimates. A similar offset between Mg/Ca and $U_{37}^{K'}$ temperatures to that found in core NIOP929 has also been documented in the North Atlantic Ocean (28–0 ka B.P. [*Elderfield and Ganssen*, 2000]) and Equatorial Atlantic Ocean (270–0 ka B.P. [*Nürnberg et al.*, 2000]).

[30] Data on the seasonal distribution of the respective proxy carriers indicate that, assuming a similar depth distribution for both proxy carriers, the calcification temperature difference is only ~0.5°C (§1.2). Using the slightly higher estimate of roughly 1°C by *Rostek et al.* [1997], the offset seen in the upper 20,000 years of Core NIOP929 may be explained. Regarding the previous glacial-interglacial transition, however, this effect is clearly insufficient to explain the larger offset.

[31] Possibly the seasonal distribution or depth habitat of the proxy carriers was different during the period152–94 ka B.P. A simple shift of the preferred calcification period of *G. ruber* to a cooler season or occurring at greater depth, however, would require a simultaneous increase in $\delta^{18}O$ values. The lighter $\delta^{18}O$ values during the interval 152–94 ka B.P. compared to the 20–0 ka B.P. interval (Figure 6) conflict such a scenario. The depth habitat of the alkenone producers has likely changed; in the modern oceans, including the Indian Ocean, alkenone production is dominated by *E. huxleyi* [*Brassell*, 1993; *Sonzogni et al.*, 1997a, 1997b]. This dominance dates back to ~80 ka B.P., before which time *G. oceanica* was the dominant alkenone producer [*Müller et al.*, 1997]. Data by *Andruleit et al.* [2003] indicate that the majority of *E. huxleyi* lives close to the thermocline, whereas *G. oceanica* occurs roughly equally distributed in the uppermost 50 m. If this difference in depth habitat between the two species is robust, the shift in dominant alkenone-producing species would result in a temperature difference of 0–1°C. The change in dominant species is reported to not have caused a change in the alkenone unsaturation-temperature relation [*Villanueva et al.*, 2002]. The depth habitat of *G. oceanica* in MIS 5e might have been shallower than today, but because of its already shallow habitat nowadays that would not have had a strong effect. The difference in temperature between the upper 50 m and the surface in CTD stations in the vicinity of Core NIOP929 is highly variable (0–2.4°C) during the summer monsoon.

[32] The seasonal distribution of the alkenone producers and their temperature recording strategies are not yet fully understood. In sediment cores, alkenones seem to document annual average SST, even though in most provinces, haptophyte production is highly seasonal [*Bijma et al.*, 2001; *Budziak et al.*, 2000; *Herbert*, 2001; *Herbert et al.*, 1998;

Nürnberg et al., 2000; *Sachs et al.*, 2000; *Sonzogni et al.*, 1997a, 1997b; *Volkman*, 2000]. In the Arabian Sea, modern coccolith/coccosphere/alkenone production is concentrated in both monsoon periods [*Andruleit et al.*, 2000; *Broerse et al.*, 2000; *Prahl et al.*, 2000]. Nevertheless, the $U^{K'}_{37}$ temperatures match annual average SST, which is higher than the upwelling-influenced monsoon season SST. If the alkenone generating biota in MIS 6 and 5 had shifted to the warmer (possibly the nonupwelling) season, they would yield $U^{K'}_{37}$ temperatures that are higher than the annual average, which could explain the observed high alkenone temperatures in the penultimate deglacial period. Although possible, such a shift to the late upwelling season, or even partially into the intermonsoon season, seems unlikely as it would place reproduction of alkenone producing species in the oligotrophic season.

5.1.2. Mg/Ca and $U^{K'}_{37}$ Offset: Possible Other Factors Causing the Temperature Offset

[33] There are several factors that could have contributed to $U^{K'}_{37}$ temperatures being higher than Mg/Ca temperature [see also *Bard*, 2001a]. We will discuss differential dissolution of foraminiferal tests, lateral transport of the alkenone-bearing fine fraction, and differential bioturbation.

[34] Preferential dissolution of high-Mg calcite could be a significant factor even though Core NIOP929 is located above the lysocline [*Conan et al.*, 2002; *Schulte and Bard*, 2003]. We use foraminiferal test weight as an indicator of carbonate dissolution [*Lohmann*, 1995; *Broecker and Clark*, 2001]. Dissolution is difficult to quantify, since most indices used (fragmentation, percentage of coarse fraction, ratio of fragile to resistant shells, etc.) reflect both dissolution and productivity. The use of foraminiferal shell weight as a dissolution index in Core NIOP929 is corroborated by the similar patterns in both shell weight and fragmentation records covering the 20–0 ka B.P. section of the core [*Saher et al.*, 2007a]. Fragmentation data for the MIS 6–5 section of Core NIOP929 is not available. The absence of clear trends in the shell weight record (Figure 3) shows no indication for significant dissolution changes over glacial-interglacial timescales. The $\sim$1 μg lower average shell weight compared with the 20–0 ka B.P. section of the same core [*Saher et al.*, 2007a] might indicate moderate, but uniform dissolution over the entire 152–94 ka B.P. interval, assuming initial shell weight remained constant (see discussion by *Barker and Elderfield* [2002]). If the dissolution correction method proposed by *Rosenthal and Lohmann* [2002] is applied to this Mg/Ca record, the discrepancy between Mg/Ca and $U^{k'}_{37}$ temperature is lowered by $\sim$1°C for MIS 6–5 and only by $\sim$0.35°C in the 20–0 ka B.P. section (Figure 4). Carbonate dissolution may thus be a partial explanation for the Mg/Ca-$U^{K'}_{37}$ offset.

[35] Lateral transport of the alkenone-bearing fine fraction has been discussed by *Benthien and Müller* [2000], *Mollenhauer et al.* [2003], and *Sachs et al.* [2000]. Coccolithophorids that are not incorporated in fecal pellets have a lower settling velocity than foraminifera because of their smaller size. This can lead to both a spatial [*Benthien and Müller*, 2000] and a temporal [*Mollenhauer et al.*, 2003] offset between the fine and coarse fraction. In Arabian Sea Core NIOP929, $U^{K'}_{37}$ temperature estimates reach values that are not representative for upwelling areas (Figures 2 and 4). It is possible that the alkenones were advected in from (nonupwelling) areas with higher SSTs, thus recording maximum tropical temperatures. An argument against the scenario of lateral transport is that, presently in the Arabian Sea, the organic flux to the seafloor occurs mainly as fecal pellets [*Roman et al.*, 2000], which have a much higher settling velocity than individual coccolithophorids.

[36] Differential bioturbation has been extensively discussed by *Bard* [2001b], *Mollenhauer et al.* [2003] and *Sachs et al.* [2000]. In cores with low (<10 cm ka^{-1}) sedimentation rate it can cause age discrepancies [*Wheatcroft*, 1992] of up to 3 ka [*Bard*, 2001b]. An age discrepancy between foraminifera and alkenones in Core NIOP929, with its mean sedimentation rate of 5.5 cm/ka for the studied interval, is thus possible. Hence, differential bioturbation, caused by the differences in size, susceptibility to dissolution, and abundance of the proxy carriers, may explain a temporal offset between events recorded in the Mg/Ca- and $U^{K'}_{37}$-based temperature records. (In the supplementary information we attempt to quantify such an offset.)[1] It would not, however, explain the consistent offset of the absolute values between the two temperature records.

[37] In summary, Mg/Ca and $U^{K'}_{37}$ data indicate a warmer MIS 5e compared to the Holocene, although absolute temperature values differ. The larger temperature discrepancy between Mg/Ca and $U^{K'}_{37}$ in the penultimate deglacial cycle compared to the last one may be partly (<1°C) due to calcite dissolution. Lateral transport of alkenone bearing fine-grained material may have contributed to the offset, but its magnitude is difficult to quantify. We have not been able to explain the high $U^{K'}_{37}$ temperatures without questioning the reliability of the Mg/Ca temperatures. This could either indicate lack of understanding of the processes leading to an originally warm signal in the $U^{K'}_{37}$ record, or to its secondary alteration. We point out that $U^{K'}_{37}$ paleothermometry may yield a much higher temperature than the flux-weighted calcification temperatures of the producing algae.

5.2. Implications of the Differences in Temperature for Core NIOP929

[38] The $U^{K'}_{37}$ record seems to represent tropical, nonupwelling temperatures at (the vicinity of) site NIOP929, suggesting these were around 26°C in the glacial and around 29°C in the interglacial period. The broad MIS 5e temperature maximum, and the absence of a temperature "shoulder" (124–117 ka B.P.) seen in the $U^{K'}_{37}$ temperature record, might be due to the finite range of the $U^{K'}_{37}$ method. The transfer function used [*Sonzogni et al.*, 1997a] does not return temperatures higher than 29.7 (at $U^{K'}_{37}$ = 1). If SST in the growing season of the coccolithophores had a similar evolution to that recorded by *G. ruber*, namely with maximum temperatures from $\sim$126 to 125 ka B.P. which are $\sim$1°C higher than temperatures in the period 124–115 ka B.P., the resulting temperatures would have exceeded the method specific SST recording capabilities, and would be improperly reflected in the downcore record.

[39] The cold event around 98 ka B.P., which is seen in the $U^{K'}_{37}$ records of both Cores NIOP929 and GeoB3005

[1] Auxiliary materials are available at ftp://ftp.agu.org/apend/pa/2007pa001557. Other auxiliary material files are in the HTML.

(Figure 5), is not reflected in the Mg/Ca temperature nor in the $\delta^{18}O$ record. An explanation for this event should be sought in a change in coccolithophorid behavior. It is possible that in this period the algae, of which even a different species may have been dominant, grew at greater depth, or in a colder (part of the) season. Alternatively, a large proportion of the alkenones may have been laterally advected from areas with stronger upwelling. Given that this cold event is documented in the $U^{K'}_{37}$ records of both cores, however, this scenario demands large-scale lateral advection as the respective sampling sites are 150 km apart.

5.3. Implications of the Differences in Timing for Core NIOP929

[40] When discussing the implications of the phasing differences in the various records, we start with the leads and lags between Mg/Ca temperature and $\delta^{18}O$, as these records are based on the same proxy carrier. The lead in Mg/Ca temperature with respect to $\delta^{18}O$ at the onset of the deglaciation (Figure 4), a phenomenon seen in many records [e.g., *Bard et al.*, 1997; *Hinrichs et al.*, 1997; *Lea et al.*, 2002; *Mashiotta et al.*, 1999; *Pichon et al.*, 1992; *Visser et al.*, 2003], illustrates that the Arabian Sea warmed before the high-latitude ice sheets started to melt. Maximum temperature was reached at 127 ka B.P., indicating that the Arabian Sea had already reached maximum temperature before the high-latitude ice sheets were reduced to minimum interglacial proportions. The drop in Mg/Ca-derived temperature at 124 ka B.P., before the end of the Termination in the $\delta^{18}O$ record, shows that the Arabian Sea even began to cool before deglacial melting was completed. Together these indicate a consistent lead of the Arabian Sea temperatures with respect to high-latitude climate change.

[41] When discussing the possible implications of the time lag of the $U^{K'}_{37}$ record relative to the Mg/Ca record, as seen at the onset of the deglacial warming, we should keep in mind that these records are based on different proxy carriers. Differential bioturbation of the proxy carriers, because of differences in size [*Bard*, 2001b], abundance [*Bard et al.*, 1987; *Hutson*, 1980] or susceptibility to dissolution [*Broecker et al.*, 1984; *Keir and Michel*, 1993] can artificially offset proxy records. Evaluating all these methods, however, indicates that the maximum contribution of bioturbation is small ($\leq$2 ka) with respect to the observed 4 ka lag (see supplementary information). An explanation of this lag could be that the seasons in which the bulk of *G. ruber* grew warmed earlier than those in which the coccolithophorids grew, provided these are not identical. Long-term change in boreal winter insolation leads spring/summer insolation [*Berger*, 1978]; therefore, an insolation driven reduction in NE monsoon could raise winter SST. If, for instance, the coccolithophorids did not grow in considerable numbers during this season while *G. ruber* did, the Mg/Ca record would show an earlier SST rise than the $U^{K'}_{37}$ record.

6. Conclusions

[42] We have presented the millennial-scale $U^{K'}_{37}$- and Mg/Ca-based temperature time series of western Arabian Sea Core NIOP929, for the period 152 ka B.P. (MIS 6) to 94 ka B.P. (MIS 5d). The glacial-interglacial warming in the $U^{K'}_{37}$ record is 2.5°C, and in the Mg/Ca record 3.5°C. The $U^{K'}_{37}$ temperatures are consistently higher than the Mg/Ca temperatures, with an average difference of $\sim$3.5°C, which is in the same range as the glacial-interglacial variability of both records. The Mg/Ca temperatures are within the range expected for an upwelling region, while the alkenone temperatures are several degrees higher, with values corresponding to modern day intermonsoon SSTs. Dissolution of foraminifera tests can account for <1 C. The change from *E. huxleyi* to shallower-dwelling *G. oceanica* as the dominant alkenone-producing species most likely forms part of the explanation. We further suggest lateral advection of alkenone-bearing material from (nonupwelling) regions with higher SST, and a change in seasonal or depth distribution of either of the proxy carriers. When interpreting $U^{K'}_{37}$-based temperature time series from MIS 5 or older, it would be advisable for regions like the Arabian Sea to assess the possibility that these do not represent annual average SST, but a higher temperature, that is closer to warm season SST. Our data gives no reason for a different interpretation of MIS 5 Mg/Ca data compared to modern data, namely that they represent the flux-weighted annual average temperature of the upper $\sim$50 m of the water column.

[43] The Mg/Ca temperature record indicates that MIS 5e was warmer by $\sim$1.5 C than the Holocene, which is more comparable to MIS 5d. Mg/Ca temperatures in glacial stages MIS 6 and MIS 2 are comparable.

[44] At the onset of the deglacial warming, the Mg/Ca temperature leads the $U^{K'}_{37}$ temperature record by 4 ka, of which maximally 2 ka may be explained by postdepositional processes. Furthermore, deglacial warming in both temperature records leads the deglacial decrease in $\delta^{18}O$, and Mg/Ca values even drop before $\delta^{18}O$ has reached minimum interglacial values. This indicates a substantial lead in Arabian Sea warming compared to global ice melting.

[45] **Acknowledgments.** The Mg/Ca measurements were made possible by the EU CESOP program. The manuscript benefited greatly from the comments of the editor and three anonymous reviewers, who are thanked for the considerable amount of time they have evidently dedicated to it. Dmitry Divine is thanked for his help with SiZer.

References

Anand, P., H. Elderfield, and M. H. Conte (2003), Calibration of Mg/Ca thermometry in planktonic foraminifera from a sediment trap time series, *Paleoceanography*, *18*(2), 1050, doi:10.1029/2002PA000846.

Andruleit, H. A., U. von Rad, A. Bruns, and V. Ittekkot (2000), Coccolithophore fluxes from sediment traps in the northeastern Arabian Sea off Pakistan, *Mar. Micropaleontol.*, *38*, 285–308, doi:10.1016/S0377-8398(00)00007-4.

Andruleit, H., S. Stäger, U. Rogalla, and P. Čepek (2003), Living coccolithophores in the northern Arabian Sea: Ecological tolerances and environmental control, *Mar. Micropaleontol.*, *49*, 157–181, doi:10.1016/S0377-8398(03)00049-5.

Bard, E. (2001a), Comparison of alkenone estimates with other paleotemperature proxies, *Geochem. Geophys. Geosyst.*, *2*(1), doi:10.1029/2000GC000050.

Bard, E. (2001b), Paleoceanographic implications of the difference in deep-sea sediment mixing between large and fine particles, *Paleoceanography*, *16*, 235–239, doi:10.1029/2000PA000537.

Bard, E., M. Arnold, J. Duprat, J. Moyes, and J.-C. Duplessy (1987), Reconstruction of the last deglaciation: Deconvolved records of $\delta^{18}O$ profiles, micropaleontological variations and accelerator mass spectrometric ^{14}C dating, *Clim. Dyn.*, *1*, 101–112, doi:10.1007/BF01054479.

Bard, E., F. Rostek, and C. Sonzogni (1997), Interhemispheric synchrony of the last deglaciation inferred from alkenone paleothermometry, *Nature*, *385*, 707–710, doi:10.1038/385707a0.

Barker, S., and H. Elderfield (2002), Foraminiferal calcification response to glacial-interglacial changes in atmospheric CO_2, *Science*, *297*, 833–836, doi:10.1126/science.1072815.

Barker, S., M. Greaves, and H. Elderfield (2003), A study of cleaning procedures used for foraminiferal Mg/Ca paleothermometry, *Geochem. Geophys. Geosyst.*, *4*(9), 8407, doi:10.1029/2003GC000559.

Benthien, A., and P. J. Müller (2000), Anomalously low alkenone temperatures caused by lateral particle and sediment transport in the Malvinas Current region, western Argentine Basin, *Deep Sea Res., Part I*, *47*, 2369–2393, doi:10.1016/S0967-0637(00)00030-3.

Berger, A. L. (1978), Long-term variations of daily insolation and Quaternary climatic changes, *J. Atmos. Sci.*, *35*, 2362–2367, doi:10.1175/1520-0469(1978)035<2362:LTVODI>2.0.CO;2.

Bijma, J., M. Altabet, M. Conte, H. Kinkel, G. J. M. Versteegh, J. K. Volkman, S. G. Wakeham, and P. P. Weaver (2001), Primary signal: Ecological and environmental factors—Report from Working Group 2, *Geochem. Geophys. Geosyst.*, *2*(1), doi:10.1029/2000GC000051.

Blanz, T., K.-C. Emeis, and H. Siegel (2005), Controls on alkenone unsaturation ratios along the salinity gradient between the open ocean and the Baltic Sea, *Geochim. Cosmochim. Acta*, *69*, 3589–3600, doi:10.1016/j.gca.2005.02.026.

Brassell, S. C. (1993), Applications of biomarkers for delineating marine paleoclimatic fluctuations during the Pleistocene, in *Organic Geochemistry: Principles and Applications*, edited by M. H. Engel and S. A. Macko, pp. 699–738, Plenum, New York.

Broecker, W., and E. Clark (2001), An evaluation of Lohmann's foraminifera weight dissolution index, *Paleoceanography*, *16*, 531–534, doi:10.1029/2000PA000600.

Broecker, W., A. Mix, M. Andree, and H. Oeschger (1984), Radiocarbon measurements on coexisting benthic and planktic foraminifera shells: Potential for reconstructing ocean ventilation times over the past 20 000 years, *Nucl. Instrum. Methods Phys. Res., Sect. B*, *5*, 331–339, doi:10.1016/0168-583X(84)90538-X.

Broerse, A. T. C., G.-J. A. Brummer, and J. E. V. Hinte (2000), Coccolithophore export production in response to monsoonal upwelling off Somalia (northwestern Indian Ocean), *Deep Sea Res., Part II*, *47*, 2179–2205, doi:10.1016/S0967-0645(00)00021-7.

Brummer, G. J. A., H. T. Kloosterhuis, and W. Helder (2002), Monsoon-driven export fluxes and early diagenesis of particulate nitrogen and its $\delta^{15}N$ across the Somalia margin, in *The Tectonic and Climatic Evolution of the Arabian Sea Region*, edited by P. D. Clift et al., *Geol. Soc. Spec. Publ.*, *195*, 353–370.

Budziak, D. (2001), Late Quaternary insolation monsoonal climate and related variations in paleoproductivity and alkenone-derived sea-surface temperatures in the western Arabian Sea, *Rep. 170*, Fachbereich Geowiss, Univ. Bremen, Bremen, Germany.

Budziak, D., R. R. Schneider, F. Rostek, P. J. Müller, E. Bard, and G. Wefer (2000), Late Quaternary insolation forcing on total organic carbon and C_{37} alkenone variations in the Arabian Sea, *Paleoceanography*, *15*, 307–321, doi:10.1029/1999PA000433.

Calvo, E., C. Pelejero, J. C. Herguera, A. Palanques, and J. O. Grimalt (2001), Insolation dependence of the southeastern subtropical Pacific sea surface temperature over the last 400 Kyrs, *Geophys. Res. Lett.*, *28*, 2481–2484, doi:10.1029/2000GL012024.

Conan, S. M.-H., and G. J. A. Brummer (2000), Fluxes of planktic foraminifera in response to monsoonal upwelling on the Somalia Basin margin, *Deep Sea Res., Part II*, *47*, 2207–2227, doi:10.1016/S0967-0645(00)00022-9.

Conan, S. M.-H., E. M. Ivanova, and G.-J. A. Brummer (2002), Quantifying carbonate dissolution and calibration of foraminiferal dissolution indices in the Somali Basin, *Mar. Geol.*, *182*, 325–349, doi:10.1016/S0025-3227(01)00238-9.

Conte, M. H., A. Thompson, D. Lesley, and R. P. Harris (1998), Genetic and physiological influences on the alkenone/alkenoate versus growth temperature relationship, in *Emiliania huxleyi and Gephyrocapsa Oceanica*, *Geochim. Cosmochim. Acta*, *62*, 51–68.

Conte, M. H., N. Ralph, and E. H. Ross (2001), Seasonal and interannual variability in deep ocean particle fluxes at the Oceanic Flux Program (OFP)/Bermuda Atlantic Time Series (BATS) site in the western Sargasso Sea near Bermuda, *Deep Sea Res., Part II*, *48*, 1471–1505.

Conte, M. H., M.-A. Sicre, C. Rühlemann, J. C. Weber, S. Schulte, D. Schulz-Bull, and T. Blanz (2006), Global temperature calibration of the alkenone unsaturation index ($U^{K'}_{37}$) in surface waters and comparison with surface sediments, *Geochem. Geophys. Geosyst.*, *7*, Q02005, doi:10.1029/2005GC001054.

Curry, W. B., D. R. Ostermann, M. V. S. Guptha, and V. Ittekkot (1992), Foraminiferal production and monsoonal upwelling in the Arabian Sea: Evidence from sediment traps, in *Upwelling Systems: Evolution Since the Miocene*, edited by C. P. Summerhayes, W. L. Prell, and K. C. Emeis, *Geol. Soc. Spec. Publ.*, *64*, 93–106.

de Villiers, S., M. Greaves, and H. Elderfield (2002), An intensity ratio calibration method for the accurate determination of Mg/Ca and Sr/Ca of marine carbonates by ICP-AES, *Geochem. Geophys. Geosyst.*, *3*(1), doi:10.1029/2001GC000169.

Eglinton, G., S. Bradshaw, A. Rosell, M. Sarnthein, U. Pflaumann, and R. Tiedemann (1992), Molecular record of secular sea surface temperature changes on 100-year timescales for glacial terminations I, II and IV, *Nature*, *356*, 423–426, doi:10.1038/356423a0.

Elderfield, H., and G. Ganssen (2000), Past temperatures and $\delta^{18}O$ of surface ocean waters inferred from foraminiferal Mg/Ca ratios, *Nature*, *405*, 442–445, doi:10.1038/35013033.

Elderfield, H., J. Yu, P. Anand, T. Kiefer, and B. Nyland (2006), Calibrations for benthic foraminiferal Mg/Ca paleothermometry and the carbonate ion hypothesis, *Earth Planet. Sci. Lett.*, *250*, 633–649.

Ferguson, J. E., G. M. Henderson, M. Kucera, and R. E. M. Rickaby (2008), Systematic change of foraminiferal Mg/Ca ratios across a strong salinity gradient, *Earth Planet. Sci. Lett.*, *265*, 153–166, doi:10.1016/j.epsl.2007.10.011.

Herbert, T. D. (2001), Review of alkenone calibrations (culture, water column, and sediments), *Geochem. Geophys. Geosyst.*, *2*(2), doi:10.1029/2000GC000055.

Herbert, T. D., J. D. Schuffert, D. Thomas, C. Lange, A. Weinheimer, A. Peleo-Alampay, and J.-C. Herguera (1998), Depth and seasonality of alkenone production along the California margin inferred from a core top transect, *Paleoceanography*, *13*, 263–271, doi:10.1029/98PA00069.

Hinrichs, K.-U., J. Rinna, J. Rullkötter, and R. Stein (1997), A 160-kyr record of alkenone-derived sea-surface temperatures from Santa Barbara Basin sediments, *Naturwissenschaften*, *84,* 126–128, doi:10.1007/s001140050361.

Hutson, W. H. (1980), Bioturbation of deep-sea sediments: Oxygen isotopes and stratigraphic uncertainty, *Geology*, *8*, 127–130, doi:10.1130/0091-7613(1980)8<127:BODSOI>2.0.CO;2.

Ittekkot, V., B. Haake, M. Bartsch, R. R. Nair, and V. Ramaswamy (1992), Organic carbon removal in the sea: The continental connection, in *Upwelling Systems: Evolution Since the Early Miocene*, edited by C. P. Summerhayes, W. L. Prell, and K. C. Emeis, *Geol. Soc. Spec. Publ.*, *64*, 167–176.

Keir, R. S., and R. L. Michel (1993), Interface dissolution control of the ^{14}C profile in marine sediment, *Geochim. Cosmochim. Acta*, *57*, 3563–3573, doi:10.1016/0016-7037(93)90139-N.

Kisakurek, B., A. Eisenhauer, J. Erez, F. Boehm, and D. Garbe-Schoenberg (2007), Controls on Mg/Ca and Sr/Ca in planktonic foraminifera: Results from culturing experiments, *Eos Trans. AGU*, *88*(52), Fall Meet. Suppl., Abstract PP31B-0419.

Lea, D., J. Bijma, H. J. Spero, and D. Archer (1999), Implications of a carbonate ion effect on shell carbon and oxygen isotopes for glacial ocean conditions, in *Use of Proxies in Paleoceanography: Examples From the South Atlantic*, edited by G. Fischer and G. Wefer, pp. 513–522, Springer, Berlin.

Lea, D. W., P. A. Martin, D. K. Pak, and H. J. Spero (2002), Reconstructing a 350 ky history of sea level using planktonic Mg/Ca and oxygen isotope records from a Cocos Ridge core, *Quat. Sci. Rev.*, *21*, 283–293, doi:10.1016/S0277-3791(01)00081-6.

Levitus, S., T. P. Boyer, and J. Antonov (1994), *World Ocean Atlas 1994*, vol. 5, *Interannual Variability of Upper Ocean Thermal Structure*, *NOAA Atlas NESDIS*, vol. 5, 176 pp., NOAA, Silver Spring, Md.

Liu, W., Z. Liu, M. Fu, and Z. An (2008), Distribution of the C_{37} tetra-unsaturated alkenone in Lake Qinghai, China: A potential lake salinity indicator, *Geochim. Cosmochim. Acta*, *72*, 988–997, doi:10.1016/j.gca.2007.11.016.

Lohmann, G. P. (1995), A model for variation in the chemistry of planktonic foraminifera due to secondary calcification and selective dissolution, *Paleoceanography*, *10*, 445–458, doi:10.1029/95PA00059.

Madureira, L. A. S., M. H. Conte, and G. Eglinton (1995), Early diagenesis of lipid biomarker compounds in North Atlantic sediments, *Paleoceanography*, *10*, 627–642, doi:10.1029/94PA03299.

Martinson, D. G., N. G. Pisias, J. D. Hays, J. Imbrie, T. C. Moore Jr., and N. J. Shackleton (1987), Age dating and the orbital theory of the ice ages: Development of a high-resolution 0 to 300,000-year chronostratigraphy, *Quat. Res.*, *27*, 1–29, doi:10.1016/0033-5894(87)90046-9.

Mashiotta, T. A., D. W. Lea, and H. J. Spero (1999), Glacial-interglacial changes in subantarctic sea surface temperature and δ^{18}O-water using foraminiferal Mg, *Earth Planet. Sci. Lett.*, *170*, 417–432, doi:10.1016/S0012-821X(99)00116-8.

McCaffrey, M. A., J. W. Farrington, and D. J. Repeta (1990), The organic geochemistry of Peru margin surface sediments: I. A comparison of the C_{37} alkenone and historical El Niño records, *Geochim. Cosmochim. Acta*, *54*, 1671–1682, doi:10.1016/0016-7037(90)90399-6.

McConnell, M. C., and R. C. Thunell (2005), Calibration of the planktonic foraminiferal Mg/Ca paleothermometer: Sediment trap results from the Guaymas Basin, Gulf of California, *Paleoceanography*, *20*, PA2016, doi:10.1029/2004PA001077.

Mix, A. C., E. Bard, G. Eglinton, L. D. Keigwin, A. C. Ravelo, and Y. Rosenthal (2000), Alkenones and multiproxy strategies in paleoceanographic studies, *Geochem. Geophys. Geosyst.*, *1*(11), doi:10.1029/2000GC000056.

Mollenhauer, G., T. I. Eglinton, N. Ohkouchi, R. R. Schneider, P. J. Müller, P. M. Grootes, and J. Rullkötter (2003), Asynchronous alkenone and foraminifera records from the Benguela upwelling system, *Geochim. Cosmochim. Acta*, *67*, 2157–2171, doi:10.1016/S0016-7037(03)00168-6.

Müller, P. J., M. Cepek, G. Ruhland, and R. R. Schneider (1997), Alkenone and coccolithophorid species changes in Late Quaternary sediments from the Walvis Ridge: Implications for the alkenone paleotemperature method, *Palaeogeogr. Palaeoclimatol. Palaeoecol.*, *135*, 71–96, doi:10.1016/S0031-0182(97)00018-7.

Müller, P. J., G. Kirst, G. Ruhland, I. von Storch, and A. Rosell-Melé (1998), Calibration of the alkenone paleotemperature index $U^{K'}_{37}$(based on core-tops from the eastern South Atlantic and the global ocean (60°N–60°S), *Geochim. Cosmochim. Acta*, *62*, 1757–1772.

Nürnberg, D., A. Müller, and R. R. Schneider (2000), Paleo-sea surface temperature calculations in the equatorial East Atlantic from Mg/Ca ratios in planktic foraminifera: A comparison to sea surface temperature estimates from $U^{K'}_{37}$, oxygen isotopes, and foraminiferal transfer function, *Paleoceanography*, *15*, 124–134, doi:10.1029/1999PA000370.

Peeters, F. J. C., G.-J. A. Brummer, and G. Ganssen (2002), The effect of upwelling on the distribution and stable isotope composition of *Globigerina bulloides* and *Globigerinoides ruber* (planktic foraminifera) in modern surface waters of the NW Arabian Sea, *Global Planet. Change*, *34*, 269–291, doi:10.1016/S0921-8181(02)00120-0.

Petit, J. R., et al. (1999), Climate and atmospheric history of the past 420000 years from the Vostok ice core, Antarctica, *Nature*, *399*, 429–436, doi:10.1038/20859.

Pichon, J.-J., L. D. Labeyrie, G. Bareille, M. Labracherie, J. Duprat, and J. Jouzel (1992), Surface water temperature changes in the high latitudes of the Southern Hemisphere over the last glacial-interglacial cycle, *Paleoceanography*, *7*, 289–318, doi:10.1029/92PA00709.

Prahl, F. G., and S. G. Wakeham (1987), Calibration of unsaturation patterns in long-chain ketone compositions for palaeotemperature assessment, *Nature*, *330*, 367–369, doi:10.1038/330367a0.

Prahl, F. G., L. A. Muehlhausen, and M. Lyle (1989), An organic geochemical assessment of oceanographic conditions at Manop Site C over the past 26,000 years, *Paleoceanography*, *4*, 495–510, doi:10.1029/PA004i005p00495.

Prahl, F. G., J. Dymond, and M. A. Sparrow (2000), Annual biomarker record for export production in the central Arabian Sea, *Deep Sea Res., Part II*, *47*, 1581–1604, doi:10.1016/S0967-0645(99)00155-1.

Roman, M., S. Smith, K. Wishner, X. Zhang, and M. Gowing (2000), Mesozooplankton production and grazing in the Arabian Sea, *Deep Sea Res., Part II*, *47*, 1423–1450, doi:10.1016/S0967-0645(99)00149-6.

Rosell-Melé, A., et al. (2001), Precision of the current methods to measure the alkenone proxy $U^{K'}_{37}$ and absolute alkenone abundance in sediments: Results of an interlaboratory comparison study, *Geochem. Geophys. Geosyst.*, *2*(7), doi:10.1029/2000GC000141.

Rosenthal, Y., and G. P. Lohmann (2002), Accurate estimation of sea surface temperatures using dissolution-corrected calibrations for Mg/Ca paleothermometry, *Paleoceanography*, *17*(3), 1044, doi:10.1029/2001PA000749.

Rostek, F., E. Bard, L. Beaufort, C. Sonzogni, and G. Ganssen (1997), Sea surface temperature and productivity records for the past 240 kyr in the Arabian Sea, *Deep Sea Res., Part II*, *44*, 1461–1480, doi:10.1016/S0967-0645(97)00008-8.

Russell, A. D., B. Honisch, H. J. Spero, and D. W. Lea (2004), Effects of seawater carbonate ion concentration and temperature on shell U, Mg, and Sr in cultured planktonic foraminifera, *Geochim. Cosmochim. Acta*, *68*, 4347–4361, doi:10.1016/j.gca.2004. 03.013.

Sachs, J. P., R. R. Schneider, T. I. Eglinton, K. H. Freeman, G. Ganssen, J. F. McManus, and D. W. Oppo (2000), Alkenones as paleoceanographic proxies, *Geochem. Geophys. Geosyst.*, *1*(11), doi:10.1029/2000GC000059.

Saher, M. H., S. J. A. Jung, H. Elderfield, M. J. Greaves, and D. Kroon (2007a), Sea surface temperatures of the western Arabian Sea during the last deglaciation, *Paleoceanography*, *22*, PA2208, doi:10.1029/2006PA001292.

Saher, M. H., F. J. C. Peeters, and D. Kroon (2007b), Sea surface temperatures during the SW and NE monsoon seasons in the western Arabian Sea over the past 20,000 years, *Palaeogeogr. Palaeoclimatol. Palaeoecol.*, *249*, 216–228, doi:10.1016/j.palaeo.2007.01.014.

Schneider, R. R., P. J. Müller, G. Ruhland, G. Meinecke, H. Schmidt, and G. Wefer (1996), Late Quaternary surface temperatures and productivity in the east-equatorial South Atlantic: Response to changes in trade/monsoon wind forcing and surface water advection, in *The South Atlantic: Present and Past Circulation*, edited by G. Wefer et al., pp. 527–551, Springer, Berlin.

Schneider, R. R., P. J. Müller, and R. Acheson (1999), Atlantic alkenone sea surface temperature records: Low versus mid latitudes and differences between hemispheres, in *Reconstructing Ocean History: A Window Into the Future*, edited by F. Abrantes and A. C. Mix, pp. 33–55, Kluwer Acad., New York.

Schott, F. A., and J. P. McCreary Jr. (2001), The monsoon circulation of the Indian Ocean, *Prog. Oceanogr.*, *51*, 1–123, doi:10.1016/S0079-6611(01)00083-0.

Schulte, S., and E. Bard (2003), Past changes in biologically mediated dissolution of calcite above the chemical lysocline recorded in Indian Ocean sediments, *Quat. Sci. Rev.*, *22*, 1757–1770, doi:10.1016/S0277-3791(03)00172-0.

Shackleton, N. J. (2000), The 100,000-year ice-age cycle identified and found to lag temperature, carbon dioxide, and orbital eccentricity, *Science*, *289*, 1897–1902, doi:10.1126/science.289.5486.1897.

Sonzogni, C., E. Bard, F. Rostek, D. Dollfus, A. Rosell-Melé, and G. Eglinton (1997a), Temperature and salinity effects on alkenone ratios measured in surface sediments from the Indian Ocean, *Quat. Res.*, *47*, 344–355, doi:10.1006/qres.1997.1885.

Sonzogni, C., E. Bard, F. Rostek, R. Lafont, A. Rosell-Melé, and G. Eglinton (1997b), Core-top calibration of the alkenone index vs sea surface temperature in the Indian Ocean, *Deep Sea Res., Part II*, *44*, 1445–1460, doi:10.1016/S0967-0645(97)00010-6.

van Hinte, J. E., T. C. E. van Weering, and S. R. Troelstra (1995), *Cruise Reports Netherlands Indian Ocean Programme*, vol. 4, *Tracing a Seasonal Upwelling*, 146 pp., Natl. Mus. of Nat. Hist., Leiden, Netherlands.

Villanueva, J., J. A. Flores, and J. O. Grimalt (2002), A detailed comparison of the $U^{k'}_{37}$ and coccolith records over the past 290 kyears: Implications to the alkenone paleotemperature method, *Org. Geochem.*, *33*, 897–905, doi:10.1016/S0146-6380(02)00067-0.

Visser, K., R. Thunell, and L. Stott (2003), Magnitude and timing of temperature change in the Indo-Pacific Warm Pool during deglaciation, *Nature*, *421*, 152–154, doi:10.1038/nature01297.

Volkman, J. K. (2000), Ecological and environmental factors affecting alkenone distributions in seawater and sediments, *Geochem. Geophys. Geosyst.*, *1*(9), doi:10.1029/2000GC000061.

Waelbroeck, C., L. Labeyrie, E. Michel, J. C. Duplessy, J. F. McManus, K. Lambeck, E. Balbon, and M. Labracherie (2002), Sea-level and deep water temperature changes derived from benthic foraminifera isotopic records, *Quat. Sci. Rev.*, *21*, 295–305, doi:10.1016/S0277-3791(01)00101-9.

Wheatcroft, R. A. (1992), Experimental tests for particle size-dependent bioturbation in the deep ocean, *Limnol. Oceanogr.*, *37*, 90–104.

E. Bard and F. Rostek, CEREGE, UMR6635, Aix-Marseille Université, IRD, Collège de France, CNRS, Europole de l'Arbois, BP80, F-13545 Aix-en-Provence, France.

H. Elderfield and M. Greaves, Department of Earth Sciences, University of Cambridge, Downing Street, Cambridge CB2 3EQ, UK.

G. M. Ganssen, Department of Paleoclimatology and Geomorphology, Institute of Earth Sciences, Vrije Universiteit Amsterdam, De Boelelaan 1085, NL-1081 HV Amsterdam, Netherlands.

S. J. A. Jung and D. Kroon, John Murray Laboratories, School of GeoSciences, University of Edinburgh, The King's Buildings, West Mains Road, Edinburgh EH9 3JW, UK.

M. H. Saher, Norwegian Polar Institute, Polar Environment Centre, N-9296 Tromsø, Norway. (margot.saher@falw.vu.nl)

R. R. Schneider, Institute of Geosciences, Christian Albrechts University of Kiel, Ludewig-Meyn-Strasse 10, D-24118 Kiel, Germany.